

# Dynamical properties of the slithering-snake algorithm: A numerical test of the activated-reptation hypothesis

L. Mattioni<sup>1</sup>, J.P. Wittmer<sup>1,a</sup>, J. Baschnagel<sup>2</sup>, J.-L. Barrat<sup>1</sup>, and E. Luijten<sup>3,4,b</sup>

<sup>1</sup> Département de Physique des Matériaux, Université Claude Bernard and CNRS, 69622 Villeurbanne Cedex, France

<sup>2</sup> Institut Charles Sadron, 6 rue Boussingault, 67083 Strasbourg, France

<sup>3</sup> Institut für Physik, Johannes-Gutenberg-Universität Mainz, 55099 Mainz, Germany

<sup>4</sup> Department of Materials Science and Engineering, University of Illinois at Urbana-Champaign, 1304 W. Green St., Urbana, IL 61801, USA

Received 18 December 2002 and Received in final form 22 March 2003 /

Published online: 12 May 2003 – © EDP Sciences / Società Italiana di Fisica / Springer-Verlag 2003

**Abstract.** Correlations in the motion of reptating polymers in a melt are investigated by means of Monte Carlo simulations of the three-dimensional slithering-snake version of the bond-fluctuation model. Surprisingly, the slithering-snake dynamics becomes inconsistent with classical reptation predictions at high chain overlap (created either by chain length  $N$  or by the volume fraction  $\phi$  of occupied lattice sites), where the relaxation times increase much faster than expected. This is due to the anomalous curvilinear diffusion in a finite time window whose upper bound  $\tau_+(N)$  is set by the density of chain ends  $\phi/N$ . Density fluctuations created by passing chain ends allow a reference polymer to break out of the local cage of immobile obstacles created by neighboring chains. The dynamics of dense solutions of “snakes” at  $t \ll \tau_+$  is identical to that of a benchmark system where all chains but one are frozen. We demonstrate that the subdiffusive dynamical regime is caused by the slow creeping of a chain out of its correlation hole. Our results are in good qualitative agreement with the activated-reptation scheme proposed recently by Semenov and Rubinstein (Eur. Phys. J. B, **1** (1998) 87). Additionally, we briefly comment on the relevance of local relaxation pathways within a slithering-snake scheme. Our preliminary results suggest that a judicious choice of the ratio of local to slithering-snake moves is crucial to equilibrate a melt of long chains efficiently.

**PACS.** 61.25.Hq Macromolecular and polymer solutions; polymer melts; swelling – 83.10.Kn Reptation and tube theories – 83.80.Sg Polymer melts

## 1 Introduction

### Background

The molecular-level description of the dynamics of non-dilute polymer liquids remains a challenging problem of great fundamental interest as well as practical importance [1]. In the last 30 years, attention has largely focused on the applicability of the *reptation* concept introduced by de Gennes and Edwards [2,3]. This approach postulates that individual chains, constrained by their neighbors, move primarily along their own contours in a snakelike fashion. Reptation-based models have been very successful in reconciling a wide range of experimental observations [1] and are broadly in agreement with more recent computational results as reviewed in [4,5].

All evidence amounts to the existence of an additional and chain-length-independent length scale. This length scale is called the “tube diameter”  $d_e \sim N_e^\nu$  with  $N_e(\phi, l_p)$  the associated “entanglement length”,  $\phi$  the molecular density,  $l_p$  the persistence length and  $\nu$  the Flory exponent of the polymer chain. The density and persistence length dependence of  $d_e$  have been probed by various numerical methods [6–10], indicating that it is proportional to the excluded-volume blob size  $\xi(\phi, l_p)$ . While, strictly speaking, not having the (more prestigious) status of a “scientific theory”, the reptation concept is widely (though not generally) seen as a physically appealing starting point any further modeling approach has to compete with.

### First motivation

The simulation of entangled polymer melts is a challenging task and it is a matter of debate if the (suspected) reptating motion of polymer chains has already been reproduced

<sup>a</sup> e-mail: [jwittmer@dpm.univ-lyon1.fr](mailto:jwittmer@dpm.univ-lyon1.fr)

<sup>b</sup> *Current address:* University of Illinois at Urbana-Champaign.

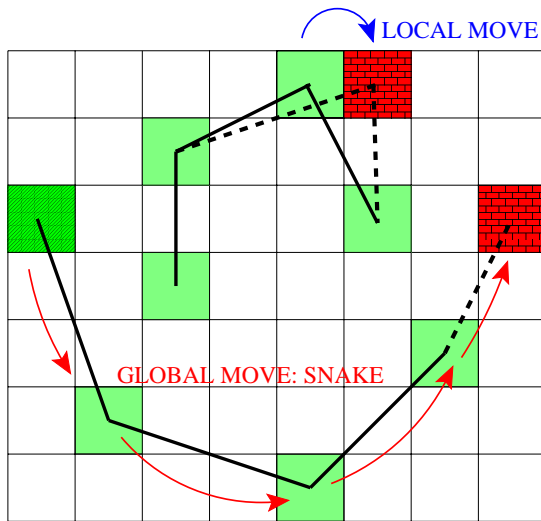


**Fig. 1.** Sketch of the bond-fluctuation model (BFM) with local (top chain) and slithering-snake moves (bottom chain). We show a two-dimensional projection of the three-dimensional Monte Carlo algorithm. Monomers (squares) are connected by 108 possible bonds (bold lines) allowing for 87 angles between bonds (in three dimensions). In the original BFM, monomers make only *local* jumps in six spatial directions, in (automatic) agreement with the imposed topological constraints. In this paper we study the dynamics of the *slithering-snake algorithm* (SSA). As depicted for the bottom chain, monomers move collectively along the chain in the SSA. Effectively, this amounts to removing a monomer (the striped one on the left), connecting it to the other end of the chain and leaving the middle monomers unchanged. Therefore, density fluctuations and constraint release only occur at the chain ends.

numerically in a sufficiently large simulation box [11]. Without any doubt, it will be near to impossible to simulate within the near future by means of *locally* realistic dynamics industrially relevant problems, such as the rheology of polymer melts with fillers. It is, therefore, tempting to accept the snakelike motion as a basic ingredient in a coarse-grained algorithm and to verify if a meaningful dynamic interpretation of the well-known “slithering-snake algorithm” (SSA) [12–14] can be given. This algorithm is sketched in Figure 1. It has been extensively used for three decades in simulations of static properties because of its efficiency in exploring phase space. Clearly, it would be extremely useful if a (simple and transparent) *mapping* of this algorithm on its corresponding local dynamical scheme could be achieved.

### Self-consistency of reptation

While most of the current computational work appears to focus on the demonstration of the curvilinear chain motion [5, 9–11, 15], here we take this key reptation hypothesis for granted. Therefore, we are not interested in the Rouse-like dynamics at short times and for chain length smaller than  $N_e$ . For the SSA we expect  $N_e \approx 1$ , so that it should be possible to explore the dynamics of the so-

called “primitive path” [3]. What we do question, however, is an additional (and arguably less profound) mean-field assumption made in the original versions of reptation which supposes the *uncorrelated* motion of neighboring “snakes”<sup>1</sup>. In the following we refer to this assumption as the “uncorrelated reptation hypothesis” (URH). One of its immediate consequences is, for instance, the linear time dependence of the mean-square displacements (MSD) of the center of mass or of the curvilinear motion of an inner chain monomer for the snake dynamics. The verification of the influence of the interchain correlations on reptating snakes is the second motivation of this study.

### Internal modes, tube fluctuations

In recent years a number of theoretical models and numerical schemes [3, 16–18] have been developed in order to explain the observed molecular-weight dependence of the zero-shear viscosity  $\eta \sim N^{3.4 \pm 0.2}$  for  $N \gg N_e$  [1, 3]. The main idea of these theories is to account for the internal modes of polymer dynamics inside the reptation tube (“tube-length fluctuations”) or to introduce a finite lifetime of the tube (“double reptation” [18]) without addressing, however, the possibility of correlated chain motion. While these are undoubtedly valiant efforts, they are of no concern here, as we are, to stress it again, interested in the physics at much larger molecular weights and correspondingly longer time scales.

### Coupling between dynamics and density fluctuations

The possibility of a coupling between primitive path dynamics and the fluctuating excluded-volume interactions of neighboring chains was first investigated by Deutsch [19]. He suggested that the reptation of a chain tail from its original tube to a new environment implies a finite free-energy penalty  $F(s)$  proportional to the curvilinear length of the tail  $s$ . Moreover, it was assumed that this additional activation energy of the snake can relax as soon as the spatial size of the escaped portion becomes of the order of the mean distance between chain ends  $d_{\text{end}} \sim N^{1/3}$ . Taking into account the Gaussian chain statistics in a dense polymer solution, Deutsch obtained an exponential increase  $\tau \sim \eta \sim N^3 \exp(N^{2/3})$  for the relaxation times and viscosities in concentrated polymer solutions with extremely large molecular masses. More recently, these ideas have been elaborated further by Semenov and Rubinstein [20–22] and implemented in a slightly different and thermodynamically fully consistent way. They predict that the URH breaks down for  $N \gg N_e^3$  [22]. Since we expect  $N_e$  to be of order 1 for the SSA, it should be possible to test this “*activated-reptation*” hypothesis (ARH) in our simulations.

<sup>1</sup> We will often use the term “snake” as a short form for “chains moving according to the slithering-snake algorithm”.

## Brief summary of our work

We have harnessed a SSA of the bond-fluctuation lattice model and compared its dynamics for consistency with the URH of the classical reptation model. We find that the dynamics rapidly slows down with chain overlap and becomes strongly subdiffusive in a finite time interval  $\tau_- \ll t \ll \tau_+$ , whose bounds are determined by the blob size  $\xi$  and the mean distance between chain ends  $d_{\text{end}}$ . This slowing-down is at variance with the URH and indicates strong correlations between neighboring chains. To corroborate our results for the SSA dynamics in an annealed molecular field, referred to as “annealed SSA” (aSSA) hereafter, we have considered a different version of the SSA where all chains but one have been quenched. We will refer to this version as the “quenched SSA” (qSSA). The comparison of both dynamical schemes demonstrates the mutual influence of the correlation hole retaining the snakes by means of an effective force and the fluctuating chain ends which allow the snakes to sneak out of the local cage of immobile monomer sites.

## Outline

This work is presented as follows. Our numerical scheme is briefly recapitulated in the next section. The parameter range and some technical points concerning the configurations and measurements are presented in Section 3. The relevant analytical predictions according to the URH and ARH are summarized in Section 4. The numerical results of this paper are presented in Section 5 where we characterize and compare aSSA and qSSA dynamics. The implications and possible extensions of our work are discussed in the final Section 6. There, we speculate on the importance of local motion to obtain a fully consistent mapping of a slithering-snake scheme on a locally realistic model.

## 2 Simulation model

### Bond-fluctuation model

In this investigation we use the extensively studied “bond-fluctuation model” (BFM) [7, 23, 24], a lattice Monte Carlo scheme introduced by Carmesin and Kremer [25]. Figure 1 depicts a two-dimensional projection of both the original BFM with local monomer dynamics (upper chain) and the BFM with global snakelike moves (lower chain). These versions have been discussed elsewhere in detail [23, 24, 26] and we concentrate here on some salient features.

In the BFM each monomer occupies the eight corners of the unit cube on a simple cubic lattice. The bonds between adjacent monomers can vary in length and direction, subject only to excluded-volume constraints and entanglement restrictions. Basically, due to the larger number of degrees of freedom—87 angles between bonds are possible—the BFM does not suffer from the same ergodicity problems that classical Monte Carlo schemes of self-avoiding random chains on simple cubic lattices are prone

to [13, 14]. (We come back to this point in Sect. 5.5.) In the original BFM version only local jumps to nearest-neighbor sites are allowed. The excluded volume then automatically forbids any intersection of bonds.

### Slithering-snake schemes: aSSA and qSSA

If snakelike moves are considered, the uncrossability of bonds has to be checked explicitly to avoid configurations which cannot be attained or unraveled by the original local scheme [27]. The snake move along the existing backbone of a chain is equivalent to removing an end monomer and connecting it to the other end of the chain, leaving the lattice positions of the middle monomers unchanged. Therefore, density fluctuations occur only at chain ends if *no* local moves are allowed.

The main focus of this study is the dynamics of the “annealed SSA” (aSSA) where all chains are allowed to move: A chain and one of its ends are selected at random and a global move in a randomly chosen bond direction is attempted. We compare this with the “quenched SSA” (qSSA) of systems where all chains but one are quenched, thus disallowing temporal density fluctuations (at chain ends or elsewhere). We sample the dynamics of the remaining free snake and average over all chains of one quenched equilibrium configuration. Unless stated otherwise, in the following we always refer to aSSA properties. Data from aSSA (qSSA) are generally indicated by open (full) symbols.

### Definition of a Monte Carlo step

Following Sokal [14] we have chosen to set the unit of the Monte Carlo time step (MCS) such that on average each monomer is attempted once per cycle, irrespective of whether this attempt occurs through local or snake moves. If only the latter are allowed, every chain is on average visited once per MCS. Our definition of the time scale differs from the one used traditionally in the description of slithering snakes, which focuses on the computational time required to equilibrate samples. Indeed every snake move requires (essentially) the same CPU time irrespective of  $N$ , since all monomers are moved simultaneously. Hence, the computational relaxation time is proportional to  $\tau_t/N$ , where  $\tau_t$  stands for the terminal relaxation time in our units.

## 3 Parameters, configurations, measurements

This section presents various technical aspects of the simulation and introduces the important static and dynamical quantities for the subsequent analysis. When a quantity is defined, we often refer to the figures where its dependence on  $N$ ,  $\phi$  or time is shown, without discussing the figure in detail, however. This discussion will be done in Section 5.

### Parameters

In this paper we study athermal systems (no additional potential parameters) containing monodisperse snakes

**Table 1.** Various static and dynamical properties for slithering snakes with aSSA dynamics at volume fraction  $\phi = 0.5$  versus chain length  $N$ : the mean bond length  $l$ , the effective bond length  $b(N) = R_e/N^{1/2}$ , the acceptance rate  $A$  (Fig. 2), the effective mobility  $m_+(N)$  from  $g_1(t)$  (Fig. 5), the spatial self-diffusion constant  $D_s = \lim_{t \rightarrow \infty} g_3(t)/6t$  (Fig. 7), the curvilinear diffusion constant  $D_c = \lim_{t \rightarrow \infty} g_6(t)/2t$  (Fig. 6) and, finally, the time scales  $\tau_1$  and  $\tau_{\text{end}}$  obtained from  $g_1(\tau_1) = R_g^2$  and  $g_1(\tau_{\text{end}}) = d_{\text{end}}^2$ , respectively (Fig. 9). The first of these times indicates the terminal time ( $\tau_1 \approx \tau_t$ ), the latter separates the strongly correlated anomalous chain diffusion from the free curvilinear diffusion at longer times ( $\tau_{\text{end}} \approx \tau_+$ ). The mean bond length  $l$  and the acceptance rate  $A$  are essentially chain length independent while the effective mobility  $m_+$  clearly is not.

$N$	$l$	$b(N)$	$A$	$m_+$	$ND_s$	$D_c$	$\tau_1$	$\tau_{\text{end}}$
16	2.602	2.9	0.08433	0.0164	0.057	0.136	299	376
32	2.603	3.0	0.08478	0.0123	0.040	0.085	1588	1257
64	2.603	3.1	0.08502	0.0071	0.022	0.045	14527	5434
128	2.603	3.1	0.08515	0.0035	0.010	0.021	$1.3 \cdot 10^5$	27826
256	2.603	3.2	0.08506	0.0012	0.0037	0.0075	$1.6 \cdot 10^6$	192900
512	2.602	3.2	0.08637	0.0003	0.0010	0.0021	$1.8 \cdot 10^7$	$0.4 \cdot 10^7$
1024	2.603	3.0	0.08606	0.0001	0.0002	0.0005	$2.5 \cdot 10^8$	$0.2 \cdot 10^8$

**Table 2.** Same properties as in Table 1, but for a lower volume fraction  $\phi = 0.125$ . Note that the effective bond length  $b(N) = R_e/N^{1/2}$  increases slightly with chain length: the chain overlap is weaker than at  $\phi = 0.5$  and larger chains are needed to screen the excluded-volume correlations. For the relatively dilute systems  $N \leq 64$  the time scale  $\tau_{\text{end}}$  becomes larger than the terminal relaxation time  $\tau_1$ .

$N$	$l$	$b(N)$	$A$	$m_+$	$ND_s$	$D_c$	$\tau_1$	$\tau_{\text{end}}$
16	2.689	3.4	0.62045	0.15	0.91	1.7	25	116
32	2.690	3.5	0.62493	0.15	0.86	1.5	94	188
64	2.691	3.7	0.62759	0.13	0.79	1.2	533	743
128	2.692	3.8	0.62888	0.11	0.66	1.0	2246	1680
256	2.692	3.9	0.62940	0.09	0.57	0.8	15142	6425
512	2.692	3.9	0.63008	0.085	0.36	0.5	94401	20059
1024	2.692	4.0	0.63006	0.055	0.28	0.3	780000	26329

(*i.e.*, disallowing any local move) at volume fractions  $\phi$  ranging from dilute solutions to dense melts ( $\phi \approx 0.5$ ). The volume fraction is defined by  $\phi = 8NN_p/L^3$ , where  $N$ ,  $N_p$  and  $L$  are the chain length, the number of polymers in the system and the linear dimension of the simulation box, respectively. In the present work, we primarily investigate the scaling of dynamical properties with mass  $N$  (see, *e.g.*, Figs. 2, 6–9, 17, 18). Chain lengths ranging from  $N = 16$  up to  $N = 1024$  have been simulated. This is sufficient to put theoretical predictions to the test. We use a periodic cubic lattice of linear size  $L = 128$ . At  $\phi = 0.5$ , this corresponds to 131072 monomers per simulation box. Note that all length scales are given in units of the lattice spacing  $a$  (*i.e.*,  $a = 1$  in the following).

In fact, we report here the first results from a larger and still on-going study, where in addition to  $N$  and  $\phi$  we have also varied the ratio  $\omega$  of local to snake moves over several orders of magnitude ranging continuously from purely local ( $\omega = \infty$ ) to pure snake dynamics ( $\omega = 0$ ). For the sake of comparison, the results of the local dynamics are included in some figures (Figs. 3, 18). At the end of this paper, we briefly comment on the influence that a finite value for  $\omega$  has on the dynamics (Fig. 18).

### Measurement of static properties

Obviously, the static properties of an ergodic system do not depend on the dynamics of the algorithm. This has

been carefully checked for the annealed SSA. (Numerically, it also appears to be true for the qSSA, even though ergodicity is less obvious in this case, since the environment of reference chains is frozen. Note, however, that all initial qSSA chains are taken from an equilibrated annealed ensemble.) This allows us to use the precise characterization obtained in previous studies, *e.g.*, for the mean bond length  $l$ , the mean end-to-end distance  $R_e$  or the mean radius of gyration  $R_g$ . The first quantity gives the mean curvilinear distance along the chain associated with every successful snake move, the second the typical displacement  $R_e/N$  of the center of mass per snake move. We recall that a polymer chain has a fractal dimension  $1/\nu$  with  $\nu$  being the Flory exponent:  $R_e \propto R_g \sim N^\nu$ . The Flory exponent for dilute chains in a good solvent is  $\nu = \nu_0 \approx 3/5$ . Above the overlap density  $\phi^* \approx N/R_g^3 \sim N^{1-3\nu_0}$ , the chains become Gaussian chains of blobs [2] with  $\nu = 1/2$ . An important length scale for the subsequent discussion is the mean distance between chain ends,  $d_{\text{end}} = (4N/\phi)^{1/3}$ , which we will often refer to as “mean end distance” in the following. Frequently, we use the “effective bond length” [3]  $b(\phi) \equiv \lim_{N \rightarrow \infty} R_e/N^{\nu=1/2}$  which is weakly density dependent. This definition is chain length independent only for systems above  $\phi^*$ . In the dilute limit, we have  $R_e/N^{\nu_0}$ , which yields  $b_0 \approx 3$  for  $N \gg 1$ . Some of these properties are summarized in Tables 1 and 2 for  $\phi = 0.5$  and  $\phi = 0.125$ , respectively. Note that  $R_g \gg d_{\text{end}} = 2N^{1/3}$  at  $\phi = 0.5$  for  $N \geq 16$ , while for  $\phi = 0.125$  chains with  $N < 64$  do not overlap,  $R_g < d_{\text{end}}$ .

### Various definitions of dynamic properties measured

As dynamical properties we have sampled various spatial and curvilinear mean-square displacements (MSD)  $g_i(t)$ , as well as associated times, diffusion coefficients and histograms. Following previous work [7], we define the *spatial* MSD  $g_1(t)$  for the middle monomer (with monomer index  $n = N/2$ ),  $g_2(t)$  for the motion of the middle monomer in the frame of the center of mass,  $g_3(t)$  for the center-of-mass motion,  $g_4(t)$  for the end monomer motion (averaged over  $n = 1$  or  $n = N$ ) and  $g_5(t)$  for the motion of the end monomers in the center-of-mass frame. Examples are given in Figures 4, 5. The MSD related to the *curvilinear* motion along the backbone is called  $g_6(t) = \langle s(t)^2 \rangle$  where  $s$  is the curvilinear distance traveled by the middle monomer  $n = N/2$  in time  $t$ . It is presented in Figures 12, 13 and 14. As we will see below, the scaling of  $g_6(t)$  and the associated histograms (see Figs. 15, 16, 17) are crucial for the understanding of the slithering-snake dynamics.

The curvilinear and spatial diffusion coefficients, presented in Tables 1 and 2 and in Figures 6, 7 and 18, are defined by  $D_c \equiv \lim_{t \rightarrow \infty} g_6(t)/2t$  and  $D_s \equiv \lim_{t \rightarrow \infty} g_3(t)/6t$ . From the diffusion coefficients we introduce the time scales  $\tau_s \equiv R_g^2/D_s$  and  $\tau_c \equiv (Nl)^2/(\pi^2 D_c)$ . The prefactor in the last definition has been introduced for convenience (see the discussion of Fig. 15 in Sect. 5.5). Additional times can be introduced to characterize the different MSDs. Following again reference [7], the time scales  $\tau_1$ ,  $\tau_2$ ,  $\tau_3$  and  $\tau_4$  are defined by  $g_1(t \equiv \tau_1) = R_g^2$ ,  $g_2(t \equiv \tau_2) = 2R_g^2/3$ ,  $g_2(t \equiv \tau_3) = g_3(t \equiv \tau_3)$  and  $g_5(t \equiv \tau_4) = R_g^2$ . In addition to this, we shall use  $g_1(t \equiv \tau_{\text{end}}) = d_{\text{end}}^2$  and  $g_1(t \equiv \tau_d) = d^2$  where  $d$  is an arbitrary distance. To characterize the curvilinear motion of the chains, we also define the time  $\tau_{N/2}$  for the diffusion of the middle monomer over half of the chain's contour by  $g_6(t \equiv \tau_{N/2}) = (Nl/2)^2$ . From the analysis it will turn out that two time scales,  $\tau_1$  and  $\tau_{\text{end}}$ , are particularly important. They have been included in Tables 1 and 2.

### Finite-size effects

Finally, we note that the results obtained for  $N = 1024$  and  $\phi = 0.5$  have to be taken with some care. The configuration contains only 128 chains and as  $L \approx R_e \approx 96$ , we cannot rule out dynamical finite-size effects —especially for the quenched SSA. Some very large motions have been observed due to chains taking advantage of the image of their own correlation hole in the neighboring periodic boxes. Unfortunately, a systematic study of the influence of the box size  $L$  is beyond our computational capabilities at present.

## 4 Analytical expectations

In the following paragraphs we summarize the relevant theoretical expectations for the analysis of the simulation data.

### Mean-square displacements: general properties

If the chains do not become permanently trapped, one expects free curvilinear and spatial diffusion, *i.e.*

$$g_6(t) \sim 2D_c t, \quad (1)$$

$$g_1(t) = g_3(t) = g_4(t) \sim 6D_s t, \quad (2)$$

for times larger than the terminal relaxation time  $\tau_t$  and for distances larger than the radius of gyration  $R_g$ . Furthermore,  $g_2$  and  $g_5$ , both defined with respect to the center of mass of the chains, must yield a purely static quantity, the radius of gyration,

$$g_2(t) \approx g_5(t)/4 \sim R_g^2, \quad (3)$$

for very long times in any ergodic dynamical scheme [8].

At short times the spatial displacement is directly expressible in terms of the curvilinear displacement  $s$  along a fractal object characterized by the Flory exponent  $\nu$ . For the MSD of the center of mass this suggests

$$Ng_3(t) \approx N \left\langle \left( \frac{\vec{R}_e s(t)}{N l} \right)^2 \right\rangle \stackrel{\text{MF}}{\approx} \frac{\langle R_e^2 \rangle}{N} \frac{g_6(t)}{l^2} \approx (b/l)^2 g_6(t), \quad (4)$$

where the penultimate step follows from a (seemingly innocent) mean-field assumption. The last step uses the fact that in the melt  $\nu = 1/2$ . For the monomer displacements along the backbone a similar reasoning gives

$$g_1(t) = g_2(t) \approx g_4(t) = g_5(t) \approx \langle R(s(t))^2 \rangle \stackrel{\text{MF}}{\approx} b^2 (g_6(t)/l^2)^\nu, \quad (5)$$

where  $\langle R(s)^2 \rangle$  is the size of a piece of chain of curvilinear length  $s$ . We have again made a mean-field approximation and assumed the fractal behavior of asymptotically long chains.

### Uncorrelated reptation hypothesis

Until now everything is fairly general and is valid for both the URH and the ARH. For uncorrelated snakes, the motion along the backbone must be linear with respect to time. This fixes the short-time predictions of the URH:

$$g_6(t) \approx 2D_c t, \quad g_3(t) \approx 6D_s t, \quad (6)$$

$$g_1(t) = g_2(t) \approx g_4(t) = g_5(t) \sim t^\nu. \quad (7)$$

Equation (6) refers, strictly speaking, to the *approximately* free diffusion along the chain backbone. As our simulation does not deal with phantom chains, there must be a small correction even for very dilute solutions. (An isolated chain is not a phantom chain. It still interacts with itself.) At long times the MSDs must obey equations (1–3).

### Activated-reptation hypothesis for a quenched molecular field

The description of the MSDs within the ARH is best outlined by considering chains in a molecular field that

is quenched at  $t = 0$  (qSSA). Hence, we start with an equilibrium ensemble of reference chains. This implies that the chains initially sit in their correlation hole with relatively low conformational free energies. To creep out of the local, well-adapted environment a free-energy penalty must be paid on average. It is then reasonable to assume [21,22] i) that fluctuations of the initial free energy may be neglected (*i.e.*, we consider a typical initial chain), ii) that the curvilinear displacement  $s$  may be taken as the *reaction coordinate* for the associated Kramers escape problem, and iii) that the same penalty  $F(s)$  may be associated with the possibly different conformations characterized by the same  $s$  —a simple, but less obvious mean-field approximation.

To estimate the dependence of the energy penalty on  $s$  it was argued in references [21,22] that  $F(s) = fs^\varphi$  for  $s \lesssim s_+(N)$  where  $f$  is a constant. The upper limit  $s_+(N)$  depends on the relaxation (escape) mechanism. Since we assumed the molecular field to be quenched, it seems natural to take  $s_+ \approx N \gg 1$ : At distances larger than the radius of gyration, translational entropy must ultimately win over all other free-energy contributions. To close the escape problem we still need to specify the physics for  $s > s_+$ . Because of the gain of the translational entropy  $F(s)$  should decrease logarithmically at large distances. A crude, but physically sufficient approximation is to relax the penalty completely:  $F(s) \equiv 0$  for  $s > s_+$  [21]<sup>2</sup>.

The exponent  $\varphi$  appears to be a matter of debate. In references [19,22] a linear relationship was suggested ( $\varphi = 1$ ). This implies that the chemical potential for a curvilinear move is constant and thus independent of the tail length  $s$ . On the other hand, it was suggested in reference [20,21] that the free-energy penalty should result from fluctuations of the molecular field rather than from a fixed chemical potential. The elaboration of this argument yields  $\varphi = 1/2$ .

Given the free-energy barrier one can calculate the mean-square displacements via equations (4, 5) if one knows the probability distribution  $p(s, t)$ . In principle,  $p(s, t)$  can be obtained from the solution of the one-dimensional Smoluchowski equation. Analytically, this calculation has not been done yet<sup>3</sup>, but the qualitative behavior of the MSDs may be inferred from the following arguments. At short times ( $t \lesssim \tau_-$ ), we have  $s \ll s_+$ , and thus  $F(s)/k_B T \ll 1$ . In this limit, one obviously recovers the free curvilinear diffusion of equations (6) and (7). If time increases, there should be an interval  $\tau_- \ll t \ll \tau_+$  such that  $k_B T \ll F(s) \ll F(s_+)$ . Here, we expect that the chain is temporally localized in its correlation hole, which should lead to a subdiffusive behavior due to intermittence of large-scale displacements. The subdiffusive regime should extend up to a “hopping time”  $\tau_+$ .  $\tau_+$  is the time taken by the chain to diffuse over the curvilinear distance  $s_+$  and thus to overcome the activation barrier.

<sup>2</sup> It is not sufficient to set  $F(s) = F(s_+)$  for  $s > s_+$  as this corresponds to a much too high return probability for the one-dimensional Kramers problem into which we have cast the original three-dimensional model.

<sup>3</sup> We determined  $p(s, t)$  in the simulations, see Figure 16.

This implies  $\tau_+ \sim s_+^2 \exp[F(s_+)/k_B T]$ . Only for  $t \gg \tau_+$  the chain can diffuse freely.

### Activated-reptation hypothesis for an annealed molecular field

Up to now, we considered the molecular field to be quenched. If all chains are allowed to move simultaneously, this annealing should reduce the activation barrier. For this case it has been suggested that  $s_+(N) \sim d_{\text{end}}^2 \sim N^{2/3}$  [19,21,22]: The free-energy constraints can be relaxed by the reptation of other chains. For short times corresponding to  $s \ll s_+$ , the difference between a quenched or an annealed molecular field should be negligible. In this limit, the correlations between neighboring chains should be essentially of static nature. On the other hand, for  $s \approx s_+$  the correlations are expected to be due to the cooperative rearrangements of several chains. Semenov and Rubinstein have proposed [22] an intricate exchange mechanism which allows the relaxation of the free-energy penalty between different snakes at  $s \approx s_+$ . It is not obvious to us if one can still cast these processes in the simple form of a one-dimensional Kramers escape problem. In any case, this should only affect the probability distributions and MSDs around  $s \approx s_+$ .

### Relaxation times and diffusion coefficients

The relative scaling of the terminal time  $\tau_t$  and the diffusion coefficients is imposed by equation (4) which fixes the ratio of both diffusion coefficients:

$$\tau_t \approx \frac{(Nl)^2}{D_c} \approx \frac{R_e^2}{D_s}. \quad (8)$$

This ensures the matching of the long- and short-time behavior. Hence,  $\tau_t(N)$ ,  $D_c(N)$ ,  $D_s(N)$  are expected to contain the same information. This should hold, irrespective of whether the URH or the ARH applies<sup>4</sup>.

As we attempt to move all  $N$  monomers of a snake collectively, the curvilinear diffusion coefficient should be independent of chain length for uncorrelated snakes. Hence, it follows from equation (8) and from the URH that

$$D_c/l^2 \approx mN^0, \quad D_s \approx m(R_e/N)^2, \quad \tau_t \approx \frac{N^2}{m}, \quad (9)$$

$m$  being the  $N$ -independent mobility which, due to the URH, should be given by the acceptance rate,  $m \approx A \sim N^0$ . Note that these equations differ by a factor of  $N$  from the usual ones characteristic of reptating chains within the URH [3]. This is due to the fact that there, a factor  $N$  is spent by the internal Rouse dynamics along the primitive path. It is precisely this missing factor which makes the

<sup>4</sup> In Section 5.3 it will be checked explicitly that this general relation still holds for the annealed SSA at different densities (Fig. 8). As we shall see, it fails, however, for the quenched SSA at high density (Figs. 11, 13).

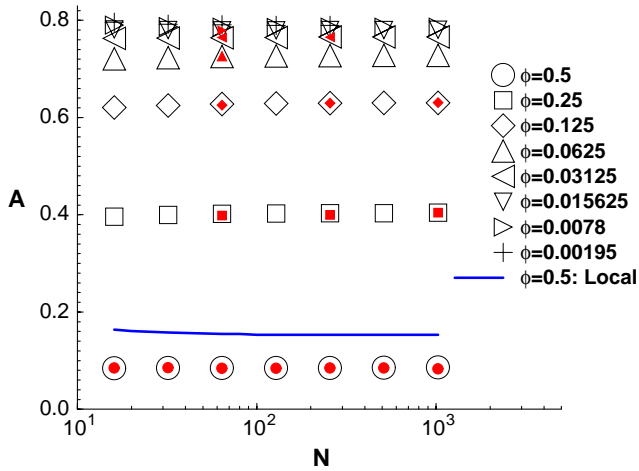


**Fig. 2.** Acceptance rate  $A$  versus  $N$  for various densities  $\phi$ , as indicated in the figure. The large open symbols correspond to the annealed SSA dynamics, while the small, filled symbols indicate the quenched SSA data. Both results are identical. For the SSA the acceptance rate is independent of chain length. Contrary to that, the bold line indicates  $A$  at  $\phi = 0.5$  for the BFM with purely local moves. Here, a slight dependence on  $N$  is found.

SSA attractive in the first place to explore the dynamics of extremely long chains.

Within the ARH the curvilinear diffusion is fixed by the hopping time  $\tau_+$  to reach a distance  $s_+$  within the potential formed by the local correlation hole, *i.e.*,

$$D_c(N)/l^2 \approx \frac{(s_+/l)^2}{\tau_+} \approx m \exp[-F(s_+(N))] = m \exp(-f s_+(N)^\varphi) \equiv m_+, \quad (10)$$

which in turn implies  $D_s(N)$  and  $\tau_t(N)$  according to equation (8). Equation (10) is obviously subject to the specific dependences of  $s_+(N)$  and  $F(s)$  on their respective parameters. We will try to estimate both  $\tau_+(N)$  and  $F(s)$  in Figures 14 and 16.

## 5 The dynamics of annealed and quenched snake fields

We begin our presentation of the slithering-snake dynamics in Section 5.1 with the characterization of local phenomenological dynamical scales. Dilute and moderately dense systems are shown in Section 5.2 to be well described by the predictions of the URH. Diffusion coefficients and characteristic time scales for a broad range of densities are presented in Section 5.3. We then focus on the dynamical properties of systems of dense solutions and melts. The various MSDs and their scaling are discussed in the next section. By analyzing various displacement histograms, possible ergodicity problems are explicitly ruled out for the annealed SSA in Section 5.5. The histograms of the curvilinear displacements allow us to estimate the free-energy penalty  $F(s)$  mentioned above.

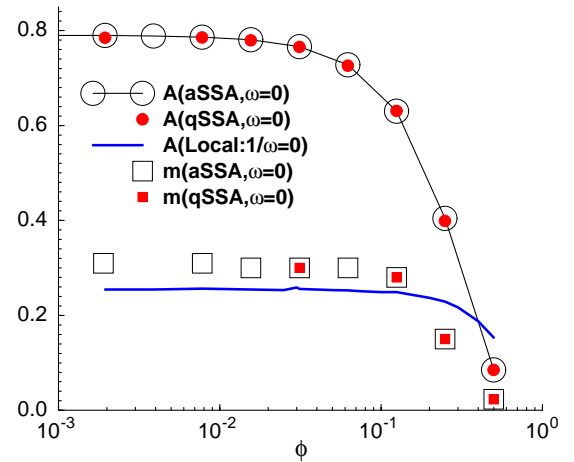


**Fig. 3.** Acceptance rate  $A$  (spheres) and local mobility  $m$  (squares) versus  $\phi$  for pure slithering-snake moves ( $\omega = 0$ ): annealed SSA (open symbols) and quenched SSA (small, filled symbols). Both  $A$  and  $m$  are not affected by the freezing of the molecular field. Also included are the acceptance rates from the BFM with local moves only ( $\omega = \infty$ ), extrapolated to infinite chain length:  $\lim_{N \rightarrow \infty} A(N, \phi)$  (bold line). For the SSA the acceptance rate and the local mobility are independent of  $N$ .

### 5.1 Local phenomenological dynamical parameters

#### Acceptance rate

The simplest and statistically most accurate dynamical property sampled in any Monte Carlo simulation is the acceptance rate  $A$  (= ratio of accepted to proposed moves). It is included in the tables and plotted *versus*  $N$  in Figure 2 and *versus*  $\phi$  in Figure 3. We note *en passant* that the acceptance rates of the aSSA and the qSSA are identical. The SSA acceptance rates are also completely independent of chain length. We recall that in contrast a weak, but systematic chain length dependence of  $A$  is found for local dynamics due to the higher mobility of the chain ends compared to inner monomers (see, *e.g.*, Fig. 10 of Ref. [7] and the bold line in Fig. 2).

As shown in Figure 3,  $A$  is density independent below  $\phi \approx 0.01$ , where it is also much larger for the SSA than for purely local dynamics. This indicates that for these densities the blob size  $\xi$  becomes sufficiently large to allow dilute SSA dynamics on distances smaller than  $\xi$ . Above  $\phi \approx 0.1$  density effects become pronounced and the acceptance rate of the SSA decreases strongly. This decrease may be explained as follows: one monomer is inserted in the SSA, *i.e.*, 8 free lattice sites are needed, whereas 4 empty sites suffice for local moves, in which a monomer is shifted from its original position by one lattice constant. Hence, the observed smaller acceptance rate for the SSA at large density ( $\phi = 0.5$ ) is expected.

#### Local mobility

Obviously, it would be naive to believe that the acceptance rate of the Monte Carlo process necessarily sets the

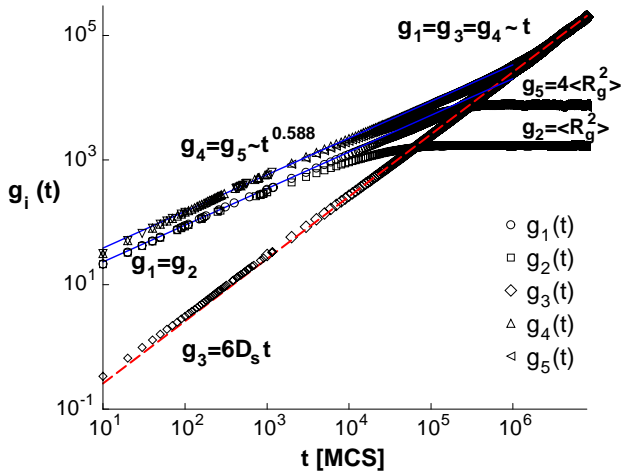


**Fig. 4.** Different spatial mean-square displacements (MSD)  $g_i(t)$  for a dilute system of chain length  $N = 512$  at volume fraction  $\phi = 0.0156$ . The MSDs are defined in Section 3. Only the data for the annealed SSA are given, as both dynamical schemes (aSSA and qSSA) yield the same results in the dilute limit. At short times,  $g_1(t) = g_2(t) \sim g_4(t) = g_5(t) \propto t^{\nu=0.588}$  (bold solid lines), as expected from equation (7). In good agreement with equation (6), we also find  $g_3(t) \propto t/N$  over (almost) the entire time range. The straight (dashed) line for  $g_3(t)$  is a fit to the long-time asymptotic limit. For large times  $g_1(t)$  and  $g_4(t)$  must merge with  $g_3(t)$ , while  $g_2(t) \rightarrow \langle R_g^2 \rangle$  and  $g_5(t) \rightarrow 4\langle R_g^2 \rangle$  converge towards time-independent static properties.

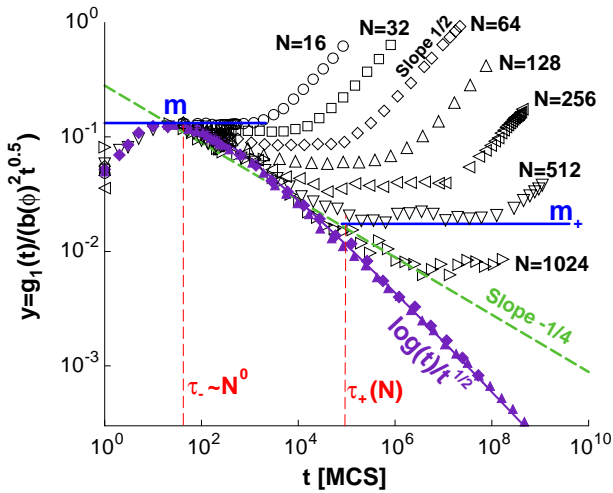


**Fig. 5.** Estimation of local and effective mobilities,  $m$  and  $m_+$ . The rescaled MSD  $y = g_1(t)/(b(\phi)^2 t^{1/2})$  for the displacements of the central monomer is shown at the melt density  $\phi = 0.5$ . The mass  $N$  varies, as indicated. Open symbols refer to the annealed SSA. We also included the qSSA results for  $N = 64$  and  $N = 128$  (filled symbols). For comparison, we show a power law with exponent  $-1/4$  (dashed line) and  $g_1(t) \approx 3.5 \log(t) - 3.8$  (bold line) which fits well the subdiffusive behavior of the qSSA. From the two horizontal envelopes of the curves we estimate the short-time mobility  $m(\phi) \sim N^0$  and the effective mobility of the snake dynamics  $m_+(N, \phi)$ . (The latter quantity is not visible for qSSA, as a much longer simulation run would have been required.) As can be seen from the figure,  $m_+$  strongly depends on chain length.

scale for the local mobility of the monomers. There may be many allowed moves not contributing to the motion. (They would also persist in a glass where the mobility is zero.) In order to measure directly the monomeric mobility  $m$  in the SSA we exploit equation (7) and compare the simulation data with

$$g_1(t) = b^2 (mt)^\nu. \quad (11)$$

This equation provides a reasonable description of the MSD of the central monomer at short times, as Figure 4 illustrates for a dilute solution and Figure 5 for a dense melt.

For dilute systems it is appropriate to fit  $g_1(t)$  using  $\nu = \nu_0$  and the density-independent effective bond length  $b_0 \approx 3$ . The same analysis can also be done in semidilute solutions for times shorter than the time required to cross the blob size so that the excluded-volume interaction is not yet screened. This approach was also applied in reference [7] to extract  $m$  for the BFM in the case when only local moves are allowed. Our results for  $m$  for both the annealed and the quenched SSA are included in Figure 3.

However, equation (11) with  $b = b_0$  and  $\nu = \nu_0$  is not the only possible way to do the analysis. For overlapping systems another choice is  $b = b(\phi)$  and  $\nu = 1/2$ . This measures the effective mobility on distances of several blob sizes. Equation (11) then suggests that  $g_1(t)$  should scale as  $g_1(t) \sim b(\phi)^2 t^{1/2}$  at short times, independent of chain length. Figure 5 confirms this expectation. If the mobility is now extracted from Figure 5, the differences between the new values and those obtained before (using  $b = b_0$  and  $\nu = \nu_0$ ) are negligible.

Here, the important point is that the local mobility is the same for all chain lengths at a given density. (Note that the mobilities obtained by Paul *et al.* [7] for the local dynamics are also independent of chain length.) Furthermore, Figures 4 and 5 also show that  $m$  is independent of whether the system is annealed (aSSA) or quenched (qSSA). For both dynamical schemes, the mobility rapidly decreases with density if  $\phi > 0.1$ . This behavior is qualitatively the same as that of the acceptance rate. Similar results are obtained if equation (11) is fitted to the MSD of the chain ends  $g_4(t)$  (not shown). For the SSA, the chain ends are more mobile than the central monomer by a factor of order one.

In summary, the acceptance rate or the local mobility cannot explain the unexpected chain length dependence of the motion of strongly entangled chains to be discussed in Sections 5.3–5.5.

### Effective mobility for the aSSA

A glance at Figure 5 shows that in fact *two* fits using equation (11) are possible for the annealed SSA once  $\phi \gg \phi^*$ . The rescaling  $y = g_1(t)/b(\phi)^2 t^{\nu=1/2}$  yields a data collapse at very short times,  $t \ll \tau_-$ . From the resulting plateau the local mobility  $m$ , shown in Figure 3, was extracted. For larger times, however,  $y$  decreases within the window  $\tau_- \ll t \ll \tau_+(N)$ . The existence of such a time window is

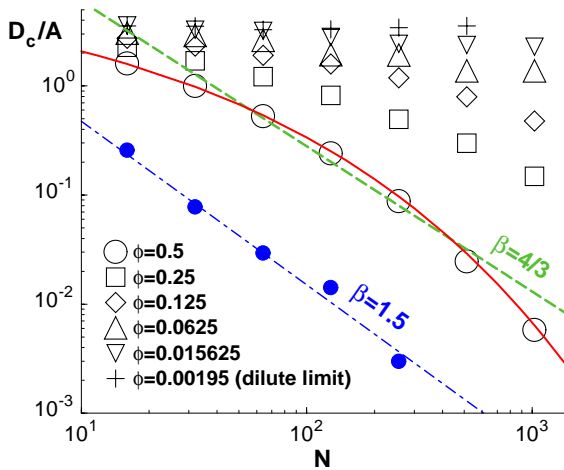


**Fig. 6.** Curvilinear diffusion coefficient  $D_c/A$  versus  $N$  for various volume fractions  $\phi$  ( $A$  = acceptance rate). The open symbols show the results for the annealed SSA, the filled symbols for the quenched SSA. Only in the dilute limit  $D_c/A \sim N^0$ , as expected. Although the effect strongly increases with  $\phi$ , we find deviations from this expectation at all densities for large chain overlap  $\phi/\phi^*(N) \gg 1$ . The effective power law with exponent  $\beta = 4/3$  roughly characterizes the chain length dependence at  $\phi = 0.5$  for the aSSA dynamics. A better fit, which properly takes into account the curvature of the data, is given by the stretched exponential  $\exp(-0.8N^{1/3})$  (bold line). The qSSA data at  $\phi = 0.5$  are well fitted by an effective power law ( $\beta \approx 1.5$ ) without any noticeable curvature (dash-dotted line).

obviously at variance with the uncorrelated reptation hypothesis. For still larger times,  $\tau_+ \ll t \ll \tau_t$ , the rescaled MSD becomes approximately horizontal. This allows us to define an *effective* mobility  $m_+(N)$  (included in the tables). It reflects the complicated correlations in the second regime  $\tau_- \ll t \ll \tau_+$ , which are responsible for its pronounced dependence on  $N$ . The importance of  $m_+$  for the description of diffusion coefficients and relaxation times will be clarified in Section 5.3. Finally, for  $t > \tau_t$ , Figure 5 shows that  $y \propto \sqrt{t}$ , implying that the monomers diffuse freely.

## 5.2 Dilute and weakly overlapping systems

Before analyzing the intricate physics at high chain overlap, we briefly consider the simpler situation of dilute or weakly overlapping solutions. These systems serve as a reference point for the following discussion of concentrated solutions and melts. That the predictions of the URH apply in the limit of high dilution can be inferred from Figures 6, 7 and 9 below. The rescaling used for the vertical axes of the three figures is motivated by equation (9) and the fact that the local mobility  $m \approx A(\phi) \sim N^0$ . The figures confirm the validity of the URH by showing that  $D_c \sim N^0$ ,  $ND_s \sim N^{2\nu_0-1}$  and  $\tau_t \approx \tau_l \sim N^2$ .

Figure 4 presents the spatial MSDs for a typical dilute or weakly overlapping configuration. We compare the measured MSDs with the expected long-time behavior

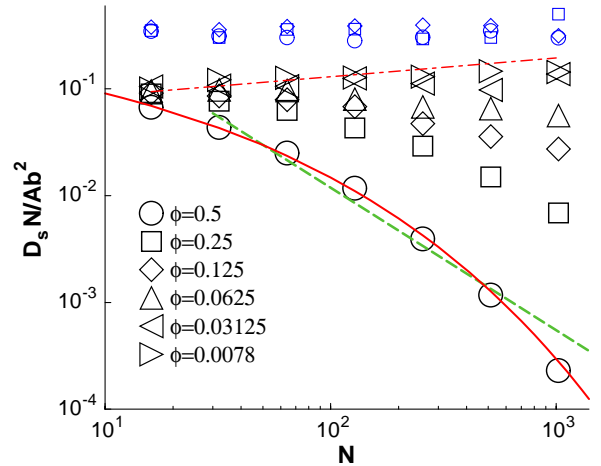


**Fig. 7.** Spatial diffusion coefficient  $D_s = \lim_{t \rightarrow \infty} g_3(t)/6t$  versus chain length  $N$  for different volume fractions  $\phi$ , as indicated in the figure (annealed SSA only). The large symbols correspond to the rescaled value  $ND_s/Ab(\phi)^2$  where we use the acceptance rate  $A(\phi) \sim N^0$  to characterize the local mobility. The small symbols (top) have been obtained by using the effective mobility  $m_+(N, \phi)$ , obtained from  $g_1(t)$  (Fig. 5), as a measure of the local mobility instead of  $A$ . The dash-dotted line corresponds to the prediction in the dilute limit,  $\beta = 1 - 2\nu_0 \approx 0.176$ . The data at  $\phi = 0.5$  are compared to the effective power law with exponent  $\beta = 4/3$  (dashed line) and the stretched exponential  $\exp(-0.8N^{1/3})$  (bold line).

(Eqs. (2, 3)) and the short-time predictions of the URH (Eqs. (6, 7) using  $\nu = \nu_0$ ). Note that the MSD of the center of mass  $g_3(t)$  is linear over several orders of magnitude, implying that corrections due to excluded-volume correlations of the snake with itself are very small. The same applies to the curvilinear motion  $g_6(t)$  (not shown). Incidentally, the excellent agreement confirms that our program is running properly and that the URH is appropriate as long as chain interactions are weak. The presented data are for the annealed SSA, but absolutely identical results have been obtained for qSSA, as expected.

The above statements remain valid for all configurations and both dynamical schemes provided that  $\phi \lesssim \phi^*$ .

## 5.3 Diffusion constants and time scales

### Diffusion coefficients for the aSSA

The curvilinear and spatial diffusion coefficients,  $D_c$  and  $ND_s$ , are displayed in Figures 6 and 7 not only for dilute solutions, but also for densities ranging up to the melt density  $\phi = 0.5$ . We plotted  $D_c/A$  and  $D_s N / Ab^2$  versus chain length, since we expected to find more or less horizontal curves (see Eq. (9)).

Surprisingly, equation (9) breaks down with increasing chain overlap. For a given density the data points become progressively curved in log-log coordinates. In fact,  $D_c$  and  $ND_s$  drop over more than two decades at  $\phi = 0.5$ , as  $N$  increases. It is important to stress that the chain length dependence of  $D_c$  and  $ND_s$  increases gradually with chain

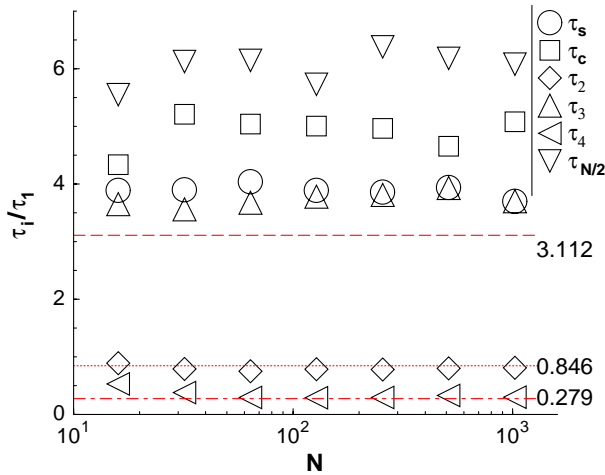


**Fig. 8.** Rescaled times  $\tau_i/\tau_1$  (defined in Sect. 3) at  $\phi = 0.5$  (aSSA only). Similar behavior is also found for other densities. This confirms that all these times are proportional to one characteristic time scale—the “terminal time”  $\tau_t$ —containing the same information as the diffusion coefficients. The horizontal lines are comparisons with the Rouse model where  $\tau_4/\tau_1 \approx 0.279$ ,  $\tau_3/\tau_1 \approx 0.846$  and  $\tau_2/\tau_1 \approx 3.112$ . Here, we did not include  $\tau_{\text{end}}$ , as its scaling is different (see Fig. 9).

overlap and that this effect is by no means a pathology of a lattice model at high density.

The data for  $\phi = 0.5$  may be compared to a phenomenological power law  $D_c \approx ND_s \sim N^{-\beta}$  with exponent  $\beta = 4/3$ . This power law is merely a guide to the eye and a rough attempt to characterize the slope in log-log coordinates for the available chain lengths. However, the stretched exponential  $D_c \approx ND_s \approx \exp(-0.8N^{1/3})$  motivated by equation (10) describes the data much better. Our scaling is, in fact, in excellent agreement with the ARH and the proposed energy barrier exponent  $\varphi = 1/2$  [21]. The alternatively suggested value  $\varphi = 1$  [19, 22] is not compatible with the simulation data (at least for the chain lengths simulated up to now).

If, instead of the acceptance rate, we use  $m_+(N)$  to rescale the diffusion coefficient, *i.e.*,  $ND_s/m_+(N)^2$ , we find a very good data collapse (small symbols at the top of Fig. 7). A similar collapse is also possible for  $D_c/m_+$  (not shown). This shows that it is possible to absorb the complicated physics at short times into one parameter,  $m_+(N)$ . Thus, the dynamics for  $\tau_+ \ll t \ll \tau_t$  is perfectly described in terms of uncorrelated reptation dynamics along the fractal chains. It remains to describe and possibly explain the dynamics in the second regime,  $\tau_- \ll t \ll \tau_+$ , of Figure 5.

#### Diffusion coefficients for the qSSA

With increasing chain overlap the qSSA diffusion coefficients decrease even more rapidly with density and chain length than their aSSA counterparts. In fact, while we have obtained most of the curvilinear diffusion coefficients from our qSSA simulations, we have been unable to mea-

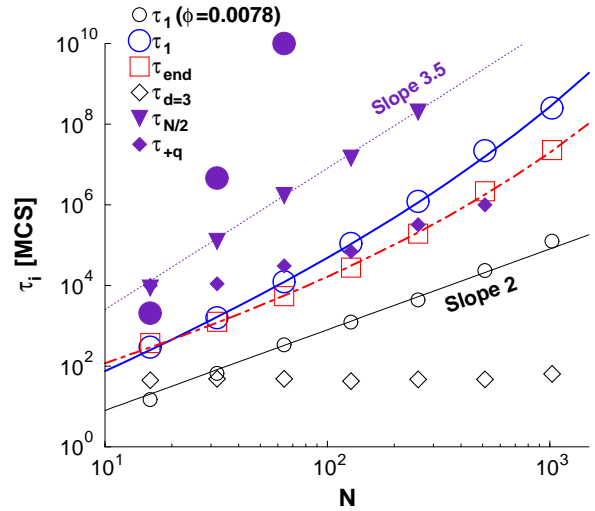


**Fig. 9.** Unscaled times *versus*  $N$ . The open symbols present the results of the annealed SSA, the filled symbols of the quenched SSA. For the aSSA dynamics  $\tau_1$ ,  $\tau_{\text{end}}$  and  $\tau_{d=3}$  (defined in Sect. 3) are shown. In the dilute limit ( $\phi = 0.0078$ ) we find  $\tau_1 \sim N^2$ , as expected (small spheres, thin line). All other data are for  $\phi = 0.5$ . The stretched exponentials are motivated by the ARH. They provide a good fit for both  $\tau_1 \approx N^2 \exp(0.8N^{1/3})$  (bold line) and  $\tau_{\text{end}} \approx N^{2/3} \exp(0.8N^{1/3})$  (dash-dotted line) at high densities. For the qSSA dynamics the filled spheres, triangles and diamonds correspond to  $\tau_1$ ,  $\tau_{N/2}$  (also defined in Sect. 3) and  $\tau_{+q}$  at  $\phi = 0.5$ .  $\tau_{+q}$  is the crossover time to free curvilinear diffusion for the qSSA (see Fig. 10 for its definition in the aSSA case). As expected, the relaxation times for the qSSA increase much faster than for the aSSA. An effective power law  $\tau_{N/2} \sim N^{3.5}$  is found in agreement with the corresponding diffusion coefficient  $D_c$  (see Fig. 6). The crossover to free curvilinear diffusion for the qSSA is roughly characterized by  $\tau_{+q} \sim N^2$  without noticeable curvature.

sure  $D_s$  for  $\phi > 0.125$ . This surprising statement is obviously at variance with equation (8). It indicates that curvilinear and spatial motions decouple for these high densities due to the localization of the snakes within their correlation hole in the quenched case. Furthermore, at high density  $D_c$  is found to be a power law without any detectable curvature (Fig. 6). However, it is interesting to check whether equation (10) with  $s_+(N) = N$  for the qSSA and  $\varphi = 1/2$  (for both schemes) yields a reasonable fit. This is indeed the case:  $D_c/A \approx 20 \exp(-0.15N^{1/2})$  is hardly distinguishable from the indicated slope  $\beta \approx 1.5$ . Longer chains are obviously necessary to confirm the exponential behavior expected by the ARH.

#### Relaxation times for the aSSA

In Figures 8 and 9 we display some of the characteristic times defined at the end of Section 3. In the first figure we test equation (8) by plotting various ratios  $\tau_i/\tau_1$ . Apparently, the ratios are independent of chain length. We find  $\tau_s/4 \approx \tau_c/5 \approx \tau_1 \approx \tau_2/0.85 \approx \tau_3/4.7 \approx \tau_4/0.3 \approx \tau_{N/2}/6$ .

Only the data for  $\phi = 0.5$  have been included, but the same results prevail for all densities. This demonstrates that all indicated times are proportional to one characteristic time scale, the “terminal time”  $\tau_t$ , containing the same information as the diffusion coefficients. That is, equation (8) still holds, although equation (9) fails.

Accordingly, Figure 9 shows, *e.g.*, that  $\tau_1$  is proportional to  $N^2$  in the dilute limit, but increases like  $\tau_1 \approx N^2/D_c \sim N^2 \exp(0.8N^{1/3})$  in the melt. The figure also includes  $\tau_d$  for  $d = 3$  and  $\tau_{\text{end}}$ . The first time indicates the distance  $d$  up to which  $g_1(t)$  remains independent of  $N$ , and characterizes the extent of the first dynamical regime displayed in Figures 5 and 12 below. In fact, it strongly decreases with monomer density, and we expect it to scale like the time needed to diffuse over the excluded-volume blob  $\xi$ . From the observed behavior of  $D_c$  one anticipates for  $\tau_{\text{end}}$  the scaling  $\tau_t \gg \tau_{\text{end}} \approx s_{\text{end}}^2/D_c \sim N^{2/3\nu} \exp(0.8N^{1/3})$ , where  $s_{\text{end}} \sim d_{\text{end}}^{1/\nu}$ . This is again consistent with the data presented in the figure.

### Relaxations times for the qSSA

Data points for  $\tau_1$  and  $\tau_{N/2}$  at  $\phi = 0.5$  have been included for the qSSA in Figure 9. Unfortunately, the range of  $N$ , which could be simulated, is insufficient to check if indeed  $\tau_1 \approx N^2 \exp(\text{const}N^{1/2})$ . The time scale  $\tau_{N/2}$ , measuring the curvilinear motion over  $N/2$  monomers, shows an effective power law which is consistent with the corresponding diffusion coefficient from Figure 6:  $\tau_{N/2} \approx N^2/D_c \sim N^{2+1.5}$ . Note that  $\tau_1$  and  $\tau_{N/2}$  scale differently in contrast to what was observed for the annealed SSA (Fig. 8).

## 5.4 Mean-square displacements of dense snakes

### Long-time limit

Focusing on systems in the melt limit ( $\phi = 0.5$ ) we now discuss several MSDs and their scaling in detail (Figs. 10–14). As a glance at the presented MSDs shows, the long-time predictions (Eqs. (1–3)) are in very good agreement with the data for the aSSA, indicating that the chains do not get trapped and that the simulation runs have been long enough. This can be seen in Figure 10 for the spatial MSDs for  $N = 512$ , in Figure 11 for both spatial and curvilinear MSDs for  $N = 128$  and in Figure 12 for the curvilinear MSD  $g_6(t)$ .

The situation is more complex for the data of the qSSA (included in Figs. 11–12). Figure 11 shows that the spatial MSDs increase (approximately) logarithmically for the longest times we have been able to simulate. This must be a transient: For very long times these MSDs must either become constant, *i.e.*, the chains become localized on a length scale (presumably) given by the radius of gyration, or ultimately, they diffuse freely in space. So far, we have been able to show conclusively only the correctness of the second proposition for small chains ( $N \leq 32$ ).

At first sight surprisingly, it is much less difficult to reach the free *curvilinear* diffusion limit, as may be seen

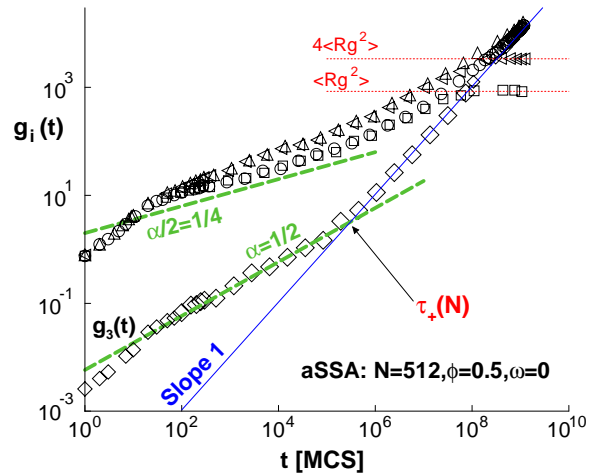


**Fig. 10.** Spatial MSDs for a dense system of chain length  $N = 512$  at volume fraction  $\phi = 0.5$  for the annealed SSA (pure slithering-snake dynamics, *i.e.*,  $\omega = 0$ ). The symbols are the same as in Figure 4. While the behavior at large times is the same as in the previous figure, much slower dynamics and strong curvature are found at short times. This is a typical result for strongly overlapping chains (either large  $\phi$  or large  $N$ ). According to equation (12), we compare  $g_1(t) = g_2(t) \approx g_4(t) = g_5(t)$  and  $g_3(t)$  with power laws characterized by an effective exponent  $\alpha = 1/2$ . The time scale  $\tau_+$  characterizes the crossover between subdiffusive and free (linear slope) center-of-mass motion. Its scaling with  $N$  is discussed in Figure 14.

from Figure 11, where  $g_6(t)$  and  $Ng_3(t)$  are directly compared for  $N = 128$ , and from Figure 12, where the  $g_6(t)$  for different masses are presented. This indicates that for the qSSA the curvilinear and spatial MSDs *decouple* for  $t \gg \tau_{\text{coup}}$  and  $s \gg s_{\text{coup}}$  (see Fig. 11); although unable to move much further in space, the snakes manage to move relatively rapidly within the cage of their correlation hole. This is why we prefer to call this surprising behavior of dense qSSA snakes (permanent or transient) *localization* in contrast to a trivial local *blocking* of the snake moves (on a scale given by the monomer density), which must obviously occur at very high densities.

### Short-time limit for the aSSA

While the MSDs are well described by the power laws of the URH in the dilute limit (Fig. 4), this becomes strikingly different at larger densities in the time window  $\tau_- \ll t \ll \tau_+$ . This is revealed by the direct comparison of dilute and dense systems with  $N = 512$ , as given in Figures 4 and 10. In this paper we attempt to characterize and to explain the features visible in the latter plot.

We have tentatively described the subdiffusive behavior of the aSSA data by means of an *effective* power law:

$$Ng_3(t) \approx g_1(t)^2 \approx g_6(t) \sim t^\alpha \text{ with } \alpha \approx 1/2. \quad (12)$$

This power law provides a remarkable fit for  $\tau_- \ll t \ll \tau_+$  (compare Figs. 5, 10, 12), even though some curvature is

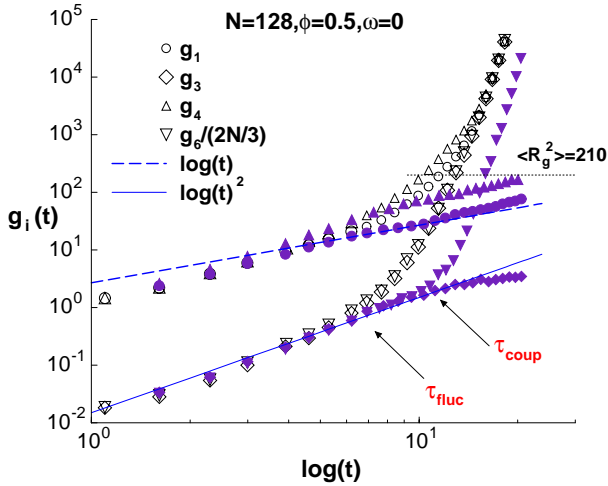


**Fig. 11.** Double logarithmic plot of spatial and curvilinear MSDs for the annealed SSA (open symbols) and the quenched SSA (filled symbols) for  $N = 128$ ,  $\phi = 0.5$  versus time. As suggested by equation (4), we rescaled the curvilinear MSD  $g_6(t)$  by  $Nl^2/b^2 \approx 2N/3$  to compare it with  $g_3(t)$ . For the aSSA spatial and curvilinear motion are coupled for all times:  $g_6(t) \sim Ng_3(t)$ . For the qSSA the run is too short to reach the spatial free diffusion limit for  $N = 128$ . However, aSSA and qSSA dynamics are identical for small times  $t \ll \tau_{\text{fluc}} \approx \tau_{\text{end}}$  (see Eq. (14)). Roughly logarithmic behavior is found for the qSSA dynamics, as indicated by the two fits  $g_1(t) \sim \log(t)$  and  $Ng_3(t) \approx g_6(t) \sim \log(t)^2$ . The time  $\tau_{\text{fluc}}$  denotes the time where the density fluctuations of the annealed field become relevant,  $\tau_{\text{coup}}$  the breakdown of the coupling of curvilinear and spatial displacements for the qSSA.

evident in log-log coordinates. The alternative fit

$$Ng_3(t) \approx g_1(t)^2 \approx g_6(t) \sim \log(t)^{4\alpha} \quad (13)$$

is less satisfactory for our aSSA data (fitting a smaller time interval), as may be seen from Figure 11. (The exponents in the two previous equations have naturally been chosen consistently with the general relationship expressed by equations (4, 5) using  $\nu = 1/2$ .)

#### Short-time limit for the qSSA

Equation (13), however, reasonably fits the qSSA data. This may be seen from Figures 5 and 11. While for the spatial MSDs this fit works for all times  $t \gg \tau_-$ ,  $g_6(t)$  becomes linear for  $t \gg \tau_{+q}$ ,  $t \gg \tau_{+a}$  with  $\tau_{+q} \gg \tau_{+a}$  (compare aSSA and qSSA in Figure 12 for  $N = 64, 128$  and  $1024$ ), where we altered the index to distinguish the different algorithms. Note that annealed SSA and quenched SSA data are identical for small times  $t \ll \tau_{\text{fluc}}(N)$  (Figs. 11,12). This is due to the low probability that a snake in the aSSA may interact with the density fluctuations created by neighboring snakes at short times. Hence, the molecular fields probed behave in the same way. As  $\tau_{\text{fluc}}(N)$  increases strongly with  $N$  (see below), this suggests that the logarithmic behavior might be seen for aSSA snakes as well, if we could simulate longer chains.

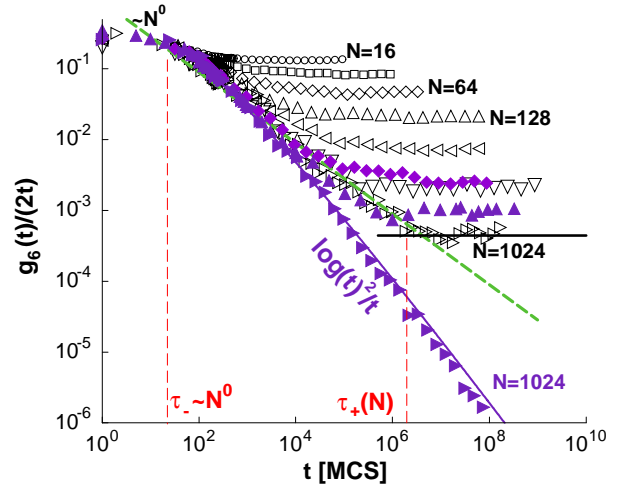


**Fig. 12.** Rescaled MSD of the curvilinear diffusion of the central monomer  $y = g_6(t)/(2t)$ . The MSD is normalized to yield the curvilinear diffusion coefficient  $D_c$  as a plateau value. The annealed SSA data (open symbols) comprise all  $N$  for the density  $\phi = 0.5$ . For comparison, we also included the qSSA results for  $N = 64, 128, 1024$  (filled symbols). At short times  $t \ll \tau_- \approx 50$ , all curves merge. For larger times the dynamics progressively slows down as a function of chain length. Only for times  $t \gg \tau_+(N)$  (indicated here for  $N = 1024$ ) we obtain the expected free curvilinear diffusion. The intermediate decrease for the aSSA dynamics is very roughly fitted by the power law  $\alpha - 1 \approx -1/2$  (dashed line). The qSSA data for  $N = 1024$  are well fitted by the logarithmic relation  $g_6(t)^{1/2} \approx \log(t)$  (bold line). This suggests that for much longer chains even the aSSA dynamics might approach this logarithmic and chain-length-independent envelope.

#### Scaling of $g_1(t)$ , $g_3(t)$ versus $g_6(t)$

In Figure 13 we verify now directly whether the time dependence of all spatial MSDs is indeed fully encapsulated in terms of the curvilinear MSD  $g_6(t)$ , as suggested by both the URH and the ARH. In the main panel of the figure we check this for the aSSA data at  $\phi = 0.5$  by plotting  $g_1(t)$  and  $g_3(t)$  versus  $g_6(t)$ . The MSD of the center of mass is linear with regard to  $g_6$ , as expected. This is in accord with the previous finding  $D_c \approx ND_s$  for Gaussian chains. We find a similar data collapse for  $g_1(g_6)$  for  $t \ll \tau_t$ . For sufficiently long chains, we clearly recover the anticipated power law of equation (7) for the diffusion on an object of inverse fractal dimension  $\nu = 1/2$  (dashed line in Fig. 13). (The departure from the slope  $1/2$  for small  $g_6(t)$  is due to the non-Gaussian statistics for small distances along the chain.) We conclude that the curvilinear and spatial diffusion are translated into each other, as expected, and that the departure from the URH can be traced back to the anomalous curvilinear diffusion depicted in Figure 12.

In the inset of Figure 13, we present  $Ng_3(g_6)$  for the qSSA for two chain lengths and two densities. While for the lower density  $g_3(t)$  remains a (roughly) linear function of  $g_6(t)$ , this is only true for short times at  $\phi = 0.5$ , where the spatial displacements increase much more strongly. Note that both densities appear to be independent of chain

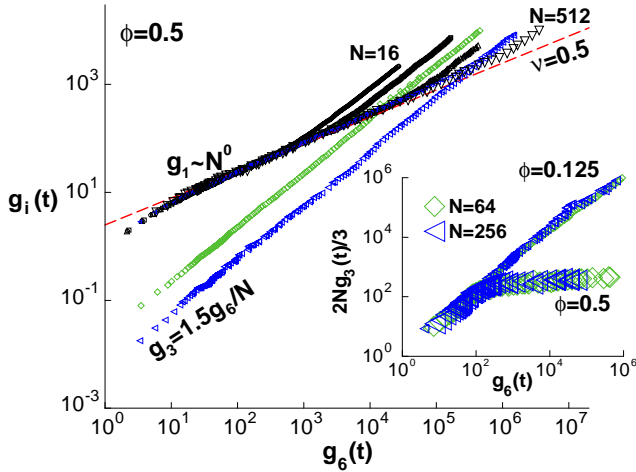


**Fig. 13.** Relative scaling of the spatial and curvilinear displacements for the aSSA (main figure) and qSSA (inset) dynamics. The MSDs are defined in Section 3. (Main figure) the spatial MSDs  $g_1(t)$  and  $g_3(t)$  are plotted *versus* the curvilinear MSD  $g_6(t)$  for various chain lengths, as indicated ( $\phi = 0.5$ ). As  $g_3(t)$  is strictly linear with respect to  $g_6(t)$  for all  $t$  and  $N$ , we only included the data for  $N = 64$  and  $N = 256$  for the sake of clarity. As expected, we find  $g_1(t) \approx b^2(g_6(t)/l^2)^{\nu=1/2} \propto N^0$  for  $t \ll \tau_t$  (dashed line labeled by  $\nu = 0.5$ ). Hence, the anticipated relations between curvilinear and spatial diffusion are verified for the aSSA dynamics and the anomalous dynamics must be fully encapsulated in terms of the curvilinear displacement  $g_6(t)$ . (Inset) rescaled spatial MSD  $2Ng_3(t)/3$  *versus*  $g_6(t)$ . Only at short times and for densities  $\phi \leq 0.125$  we find both quantities to be equal. The curvilinear motion *decouples* from the spatial motion for larger densities, where the snakes become *localized* within the correlation hole.

length. This indicates a very weak mass dependence for  $s_{\text{coup}}$ .

### Scaling with chain length

We now discuss in more detail the chain length dependence of the subdiffusive behavior at fixed volume fraction  $\phi = 0.5$ . Since we have shown (Fig. 13) that the spatial MSDs of the annealed SSA scale in terms of  $g_6(t)$ , we can concentrate on the  $N$ -dependence of the latter quantity (Fig. 12). The vertical axis is normalized to yield the curvilinear diffusion coefficient  $D_c$  as the plateau value for long times. At short times  $t \ll \tau_- \approx 50$ , all curves merge. Hence,  $\tau_-$  is chain length independent, but depends weakly on the density, as may be shown by a similar plot containing data for different  $\phi$ . For times beyond  $\tau_-$  the dynamics slows down more and more until it reaches the plateau of free diffusion at  $\tau_{+a}(N)$  for aSSA and  $\tau_{+q}(N)$  for qSSA, respectively. Apparently, the correlations become more and more pronounced with increasing  $N$ .

We have directly computed the four times  $\tau_{+a}$ ,  $\tau_{+q}$ ,  $\tau_{\text{fluc}}$  and  $\tau_{\text{coup}}$  and the related curvilinear displacements. Our measurements are not very precise (particularly, for the qSSA data better statistics is needed), and we only present some general trends here. A comparison of all

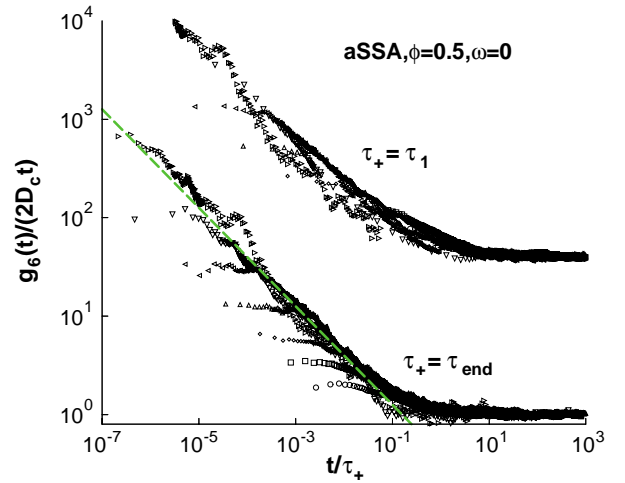


**Fig. 14.** Scaling attempts for  $g_6(t)$  in order to determine the time scale at which the curvilinear dynamics (for the aSSA) becomes freely diffusive. The natural attempt  $\tau_+ = \tau_1$  (shifted for clarity) fails. In contrast, the scaling  $\tau_+ = \tau_{\text{end}}$  is successful, demonstrating that there is an additional characteristic time related to the density of chain ends. The power law with exponent  $\alpha \approx 1/2$  for the envelope is indicated (dashed line).

chain lengths shows that

$$\tau_{\text{fluc}}(N) \approx \tau_{+a}(N) \approx \tau_{\text{end}}(N), \quad (14)$$

$$\tau_{\text{coup}}(N) \approx \tau_{+q}(N) \sim N^2. \quad (15)$$

In other words, both pairs of time scales correspond to different definitions of the same physical processes. In the first case, these are the density fluctuations in the annealed scheme, causing aSSA and qSSA to differ and the curvilinear motion to become eventually diffusive. The second equation corresponds to the free curvilinear diffusion of the snake trapped in its quenched correlation hole. The power law indicated in equation (15) is an estimate motivated by the data given in Figure 9 (diamonds).

The last claim of equation (14), which is central to the understanding of the observed correlations and is in line with the ARH [19,22], is further tested in Figure 14. The attempt  $\tau_{+a} \approx \tau_1$  fails to scale the crossover regime between the subdiffusive time window and the free curvilinear diffusion at late times. (Note that there is always the time scale  $\tau_- \sim N^0$  for the free diffusion at very short times and no scaling covering all regimes is possible.) Instead, the alternative  $\tau_{+a} \approx \tau_{\text{end}}$  is successful. The observed scaling confirms equation (14) and demonstrates that the crossover from correlated to mean-field behavior is determined by  $d_{\text{end}}$ .

Finally, we note for the second, less important, relaxation process for the qSSA that  $s_{+q}$  increases very weakly with mass,  $s_{+q}^2 \sim N^{0.25}$ . (However, this does not contradict the scaling documented in the inset of Figure 13. Note also that this is again a rough estimate, but we definitely have to rule out the two “natural” guesses  $s_{+q} \sim N$  or  $s_{+q} \sim N^0$ .) Interestingly,  $s_{+q}^2 \sim N^{0.25}$  and  $\tau_{+q}(N) \sim N^2$  are compatible with the (very precisely measured) qSSA diffusion coefficient from Figure 6,

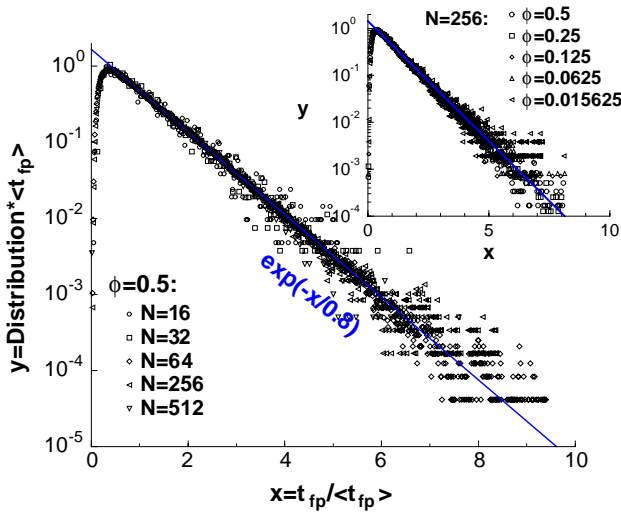


**Fig. 15.** Distribution of the first-passage time  $t_{fp}$  required to reach a curvilinear distance  $Nl/2$ . We consider aSSA systems at  $\phi = 0.5$  (main figure) and at chain length  $N = 256$  (inset). Symbols are indicated in the figure. The data points of all systems  $(\phi, N)$  collapse on the same master curve if rescaled by the mean first-passage time  $\tau_{fp} \equiv \langle t_{fp} \rangle$ . At large times the histograms decrease exponentially according to  $\exp(-t/\tau_c)$ , as expected.

$D_c \approx s_{+q}^2/\tau_{+q} \sim 1/N^{1.5}$ , and, hence, with the time scale  $\tau_{N/2} \sim N^{3.5}$  shown in Figure 9. While this is satisfactory, we presently cannot explain the scaling behavior of  $\tau_{+q}$  and  $s_{+q}$ .

## 5.5 Histograms and non-Gaussianity

So far, we have discussed results obtained from the sampled mean-square displacements and related diffusion constants and time scales. We now turn to the additional information contained in the histograms and higher moments of the *curvilinear* displacements. Merely results from the annealed field dynamics are discussed here, since statistics is too poor for the qSSA.

An important, not only technical, question concerns the possibility that some chains or monomers become locally completely blocked. We have paid much attention to this issue and have carefully checked that, in fact, all chains and monomers ultimately move arbitrarily far in space for the densities studied ( $\phi \leq 0.5$ ). Clearly, for some higher density this must eventually break down.

One may readily construct by hand chain configurations of the BFM, which lead to blocked chains for any dynamical scheme under consideration, even if local moves are allowed. These extremely rare points of the phase space also exist for our slithering-snake scheme, although they are apparently excluded from our initial configurations (which is the physically important point to make here). These states cannot be accessed (by construction) and in this strict mathematical sense our dynamics is not

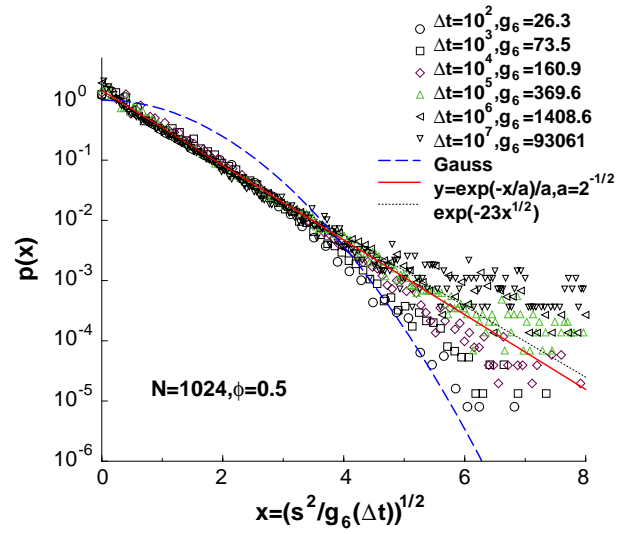


**Fig. 16.** Normalized histograms of the curvilinear motion (aSSA data only) for  $N = 1024$ ,  $\phi = 0.5$  and for different time intervals  $\Delta t$ , as indicated in the figure. The histograms are rescaled in such a way that all data should collapse if they were self-similar for all times. We show that the histograms are approximately exponential within the time interval  $\tau_- \approx 50 \ll t \ll \tau_+ = \tau_{end}(N = 1024) \approx 0.2 \cdot 10^8$ . The histograms become Gaussian again at much longer times.

ergodic. However, this is completely irrelevant for the thermodynamic and dynamic behavior<sup>5</sup>.

## Histogram of first-passage time

Two checks are presented in the histograms given in Figures 15 and 16. The first figure presents the histograms of first-passage times of the central monomer over a curvilinear distance  $s = lN/2$  for various chain lengths and densities. At long enough times, typically  $10 \tau_{fp}$ , where  $\tau_{fp} = \langle t_{fp} \rangle$  is the mean first-passage time, all chains have crept out of their initial tube. If properly rescaled, the data collapse onto a master curve. The distribution of the first-passage times can be calculated if free curvilinear diffusion is assumed. It is a linear superposition of modes  $p$  with an exponential time dependence  $\exp(-p^2 t_{fp}/\tau_c)$ . For long times, this sum is dominated by the lowest mode and, accordingly, we find an exponential decrease  $\exp(-t_{fp}/\tau_c)$  for all systems. As expected, the mean first-passage time scales like the terminal time,  $\tau_{fp} \approx 6\tau_1 \approx 5\tau_c/6$ , and is of the same order as  $\tau_{N/2}$  which was defined as the time where  $g_6(t)$  corresponds to the same curvilinear distance.

<sup>5</sup> In this context it is also of relevance that one obtains the same dynamics if a small amount of local hopping moves,  $\omega \ll 1$ , is included in the algorithm which allows additional transitions between points of the phase space. See Figure 18 below.

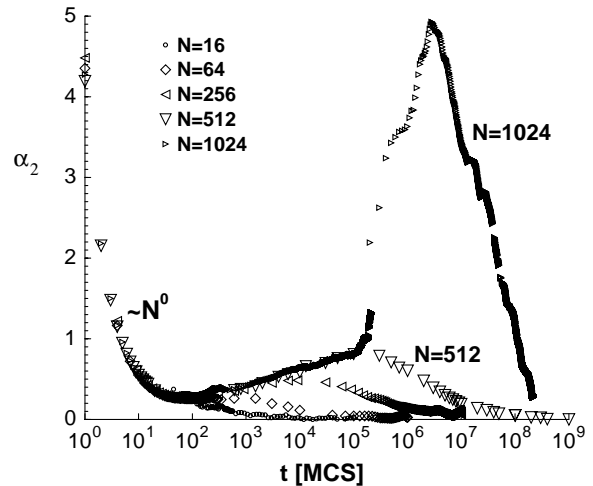
### Histogram of curvilinear displacements $s$

Figure 16 presents the histogram of  $s(\Delta t)$  for  $N = 1024$  and  $\phi = 0.5$  for various time intervals, as indicated. We focus on the interesting time window  $\tau_- \ll t \ll \tau_+ \ll \tau_t$ . First of all, we stress that the histograms have (very qualitatively) the same shape and fall off monotonously without any singularity at the origin or elsewhere, *i.e.*, no snake gets blocked at small  $s$ . If no correlations were present, the rescaled histograms should all collapse onto a single Gaussian. More importantly, however, Figure 16 shows that the different dynamical regimes correspond to (slightly) different distributions. While at times  $t \ll \tau_-$  and  $t \gg \tau_+$  ( $N = 1024$ )  $\approx 0.2 \cdot 10^8$  the distributions are in fact Gaussian<sup>6</sup>, they are essentially *exponential* in the subdiffusive regime where density fluctuations are important. The distribution is thus much *broader* than originally expected, but all moments of the distribution exist. Although this is not an equilibrium distribution measuring directly the free energy as a function of  $s$ , the Smoluchowski equation suggests that  $-\log(p(s))$  should be proportional  $F(s)$ . We have therefore compared the two proposed exponents for the activation penalty  $\varphi = 1$  (bold line) and  $\varphi = 1/2$  (dots) with the data. Unfortunately at large  $s$ , the statistics becomes too poor to distinguish between both exponents. More work is required to relate the form and scaling of the observed histograms to the respective MSD.

### Non-Gaussian parameter

The non-Gaussian parameter  $\alpha_2 \equiv \frac{1}{3} \frac{\langle s^4 \rangle}{\langle s^2 \rangle^2} - 1$  gives a compact means to describe the Gaussianity of these distributions as a function of time. This is presented in Figure 17. We recall that  $\alpha_2 = 0$  for a Gaussian and  $\alpha_2 = 1$  for an exponential distribution. At short times  $\alpha_2(t)$  decreases rapidly and is chain length independent. The non-Gaussianity at these times is due to local monomer interactions. In agreement with the histograms shown in Figure 16,  $\alpha_2(t)$  *increases* strongly for larger times. This shows again that correlations become more pronounced. The effect increases strongly with chain length in agreement with the subdiffusive behavior in Figure 12. Note that  $\alpha_2$  becomes even much larger than 1 for our largest chain  $N = 1024$ , reflecting the existence of a broad tail in the distribution shown in Figure 16. We caution, however, that finite-size effects might contribute to this effect, as the end-to-end distance of this configuration is comparable to the box size. It is possible that some snakes manage to find their way rapidly through the periodic box by taking advantage of their own groove spanning the box. For times larger than  $\tau_+(N)$  the non-Gaussianity vanishes again for all  $N$ , as it should.

<sup>6</sup> For clarity, both regimes are not included in the figure. Note that Gaussian behavior is only found in the first regime at much smaller densities than the one discussed in Figure 16. A sufficiently large blob is required to obtain a Gaussian distribution.



**Fig. 17.** Non-Gaussian parameter  $\alpha_2 \equiv \frac{1}{3} \frac{\langle s^4 \rangle}{\langle s^2 \rangle^2} - 1$  for the curvilinear displacement  $s$  of the central monomer *versus* time for  $\phi = 0.5$  and chain lengths as indicated in the figure. We find that  $\alpha_2$  becomes non-monotonous for  $\tau_- \ll t \ll \tau_+$ . Unfortunately, the statistics is poor for large  $N$  and some binning is necessary. Only the aSSA data are shown, the statistics is not sufficient for the qSSA.

## 6 Summary and outlook: snake versus local moves

### Summary

In this paper we reported first numerical results on the dynamics of monodisperse polymer chains moving according to the slithering-snake algorithm SSA (no local relaxation pathways). The simulations were done with the three-dimensional bond-fluctuation model (BFM). We investigated two different dynamical schemes by focusing mainly on the polymer melts (high monomer densities): Either we allow all snakes to move (aSSA), which permits fluctuations of the molecular field at the ends of neighboring chains, or all snakes but one are quenched (qSSA). This work concentrates on the annealed algorithm, whereas the second mainly serves as a benchmark to investigate the role of density fluctuations due to neighboring chains. We studied the scaling of various spatial and curvilinear mean-square displacements (MSD), diffusion coefficients and relaxation times with chain length. Furthermore, we also presented the distributions of the curvilinear motion.

Our results are broadly in agreement with the “activated-reptation” hypothesis (ARH) [19,22]. For the aSSA, we find that at high chain overlap the terminal relaxation time  $\tau_t$  increases much more strongly with chain length  $N$  than possible for uncorrelated snakes which are obtained for dilute and weakly overlapping chains. In fact, a stretched exponential  $\tau_t \approx N^2 \exp(0.8N^{1/3})$  fits our data well. Similar and directly related (Eq. (8)) behavior can be found for the spatial and curvilinear diffusion coefficients,  $ND_s \approx D_c$ , and other time scales, such as  $\tau_{\text{end}}$ , which measures the time needed for the diffusion over the mean distance between chain ends  $d_{\text{end}}$ . The stretching exponent  $1/3$  is in agreement with the free-energy penalty

$F(s) \sim s^{1/2}$  ( $s$  being the curvilinear displacement) estimated in reference [21], but is incompatible with the more recent suggestion  $F(s) \sim s$  of reference [22] (at least for the chain lengths accessible in the present simulation).

A more detailed study of different moments of the displacements shows that the snake dynamics is only uncorrelated (exhibiting a free curvilinear diffusion with Gaussian distribution) for times smaller than  $\tau_-(\phi) \sim N^0$ , which is determined by the blob size  $\xi$ , and for times larger than  $\tau_+ \approx \tau_{\text{end}}$  (shown by the scaling collapse of Fig. 14), which is due to the density fluctuations present for distances larger than  $d_{\text{end}}$ . They are responsible for an additional time scale (other than the terminal time) in the annealed algorithm, allowing the chains to relax the free-energy penalty caused by their motion in a locally rigid and frozen network of obstacles retaining them in their correlation hole. This is supported by the finding that the MSDs of both the aSSA and the qSSA, which are strictly identical at small times, become different around  $\tau_+$ .

In the intermediate time interval the dynamics becomes increasingly subdiffusive and non-Gaussian (Figs. 16, 17), as the chain length is increased for both aSSA and qSSA dynamics. The precise description of the MSDs in this regime is not evident for the masses we have been able to simulate and our study is not fully conclusive. While power laws yield nominally better fits for aSSA, logarithmically slow relaxation processes might also be appropriate. The observed behavior for the quenched dynamics (Figs. 11, 12), which could provide an “envelope” that the annealed dynamics might follow more closely with increasing chain length, is indeed better described in this way. Logarithmic behavior is, however, not easily reconciled with (mean-field) ARH approach which predicts an algebraic relationship. More simulations are warranted to clarify this issue.

The curvilinear displacement histograms decrease monotonously without any singularity at small  $s$ . In the subdiffusive intermediate time they decrease essentially exponentially (Fig. 16). This suggests that the free-energy penalty  $F(s)$  is indeed of power law form. A direct measurement of the acceptance rate to perform a step  $s \rightarrow s+1$  is currently underway using the quenched scheme which should allow a direct computation of the free-energy cost for an escape attempt of order  $s$ .

In summary, we believe that our study demonstrates that the activated-reptation approach is relevant for the description of concentrated solutions and melts of purely slithering snakes without local motion ( $\omega = 0$ ).

### The mapping onto a locally realistic model

It is important to recall that the slithering-snake dynamics discussed in this paper is highly artificial, as no local rearrangements are allowed and density fluctuations can only occur at chain ends. The idea is that the snake corresponds to the primitive path of the reptation model and each monomer to a coarse-grained tube segment of an originally local model. The mapping of both levels of description is non-trivial. It is not evident whether it can be

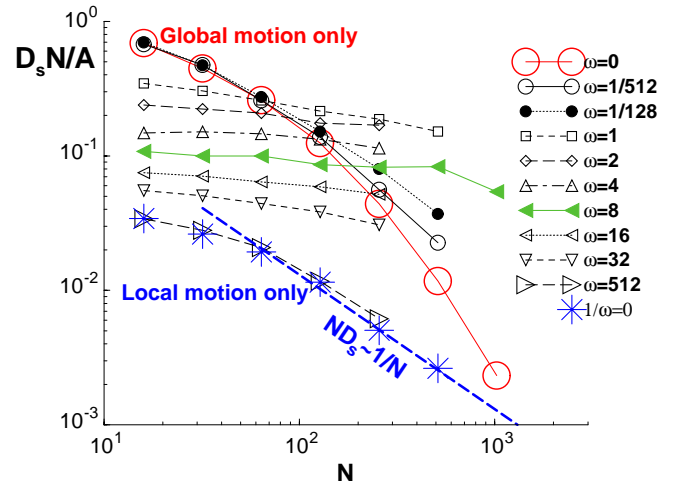


**Fig. 18.** Spatial diffusion coefficient  $ND_s$  versus  $N$  for different  $\omega$  as indicated in the figure (aSSA only):  $\omega = 0$  corresponds to pure slithering-snake dynamics,  $1/\omega = 0$  (large asterisks) to the pure local dynamics. The data for  $\omega \ll 1$  are very similar to the pure slithering-snake limit. For  $\omega \approx 8$ , equation (9) is approximately satisfied. This may define a reasonable “starting point” for future SSA simulations corresponding to the classical URH reptation approach. For the local dynamics the power law prediction  $D_s \propto 1/N^2$  (dashed line) from classical reptation theory is indicated. The data for  $\omega = 512$  approximate the local dynamics limit rather well for the chain lengths we have been able to simulate.

performed at all without an additional tuning parameter, such as the frequency of local hopping moves.

The mapping might involve the density. It is possible that some of the high molecular densities, which we studied here, are in fact too large to correspond to realistic volume densities of an underlying microscopic model. A characteristic density might therefore exist below which even asymptotically long snakes remain uncorrelated. At present, our computational results do not seem to favor this option, as suggested, *e.g.*, by Figure 7. However, it remains a possibility which is currently pursued using lower densities and much larger chains such that  $1 \gg \phi \gg \phi^*(N)$ . In any case, a more detailed analysis of the density dependence is warranted to establish the scaling of  $\tau_-(\phi)$  and  $\tau_+(N, \phi)$ . In other words, it has to be confirmed unambiguously that the first time scale is related to the blob size  $\xi(\phi)$  and the second one to the mean distance between chain ends  $d_{\text{end}}(N, \phi)$ .

### On the importance of local motion

Another issue is related to the fact that our slithering snakes do not have any mechanism to relax constraints via local pathways. It might well be that some local dynamical degrees of freedom are necessary to *tune* a mesoscopic computation scheme such that it becomes consistent with real reptational dynamics. A finite fraction of local moves should weaken the strength of the obstacles imposed by neighboring chains. This is indeed borne out by preliminary studies presented in Figure 18, where the rescaled

spatial diffusion coefficient is plotted for various ratios of local to snake moves  $\omega$ . For short chains ( $N < 64$ ),  $ND_s$  decreases monotonously with increasing  $\omega$ , since local moves are less efficient in exploring the phase space and the confinement is negligible. As the mass increases, we find a striking *non-monotonous behavior*. The dynamics first becomes more rapid, as local dense fluctuations become more relevant. This effect apparently saturates at a frequency of order 10, which causes the diffusion coefficient to decrease again strongly with increasing  $\omega$  (at fixed  $N$ ). A finite  $\omega$  generates a lateral tube of size  $d_1(\omega, \phi) > a$ , which should become identical to the tube diameter  $d_e(\phi)$  of the reptation model in the limit of very large  $\omega$ . Recalling that  $d_e(\phi) \approx \xi(\phi)$  we speculate that a successful mapping of a SSA scheme on a local scheme may require the tuning of the ratio  $d_1(\omega, \phi)/\xi(\phi) = \text{const} \approx 1$ , which implies a different  $\omega$  for each density. We are currently pursuing further simulations to clarify these questions.

### A final word

It might well turn out that even in this larger modeling space no  $\omega(\phi)$  can be found, where  $D_c \approx ND_s$  remains chain length independent for large  $N$ . We would regard this as a strong evidence for the correctness of the ARH for a model with fully realistic local dynamics. We believe, however, that astronomically long chains are required to obtain measurable effects.

During the course of this work, we had valuable discussions and obtained insights from many colleagues, especially from M. Müller, A. Johner, M. Fuchs, A.N. Semenov and S. Obukhov. LM and JPW acknowledge computational support by IDRIS/France. EL acknowledges support through a fellowship from the Max Planck Institute for Polymer Research (Mainz, Germany).

### References

1. T.P. Lodge, N.A. Rotstein, S. Prager, *Adv. Chem. Phys.*, **LXXIX**, 1 (1990).
2. P.G. de Gennes, *Scaling Concepts in Polymer Physics* (Cornell University Press, Ithaca, 1979).
3. M. Doi, S.F. Edwards, *The Theory of Polymer Dynamics* (Clarendon Press, Oxford, 1986).
4. K. Binder, W. Paul, *J. Polym. Sci.* **35**, 1 (1997).
5. K. Kremer, G.S. Grest, in *Monte Carlo and Molecular Dynamics Simulations in Polymer Science*, edited by K. Binder (Oxford University Press, New York, 1995) pp. 194-271.
6. J. Baschnagel *et al.*, *Adv. Polym. Sci.* **152**, 41 (2000).
7. W. Paul, K. Binder, D. Herrmann, K. Kremer, *J. Phys. II* **1**, 37 (1991).
8. W. Paul, K. Binder, D. Herrmann, K. Kremer, *J. Chem. Phys.* **95**, 7726 (1991).
9. M. Müller, J.P. Wittmer, J.-L. Barrat, *Europhys. Lett.* **52**, 406 (2000).
10. R. Faller, F. Müller-Plathe, *J. Chem. Phys.* **3**, 180 (2001).
11. M. Pütz, K. Kremer, G.S. Grest, *Europhys. Lett.* **49**, 735 (2000).
12. A.K. Kron, *Polym. Sci. USSR* **7**, 1361 (1965).
13. F.T. Wall, F. Mandel, *J. Chem. Phys.* **63**, 4592 (1975); F.T. Wall, J.C. Chin, *J. Chem. Phys.* **66**, 3143 (1977).
14. A.D. Sokal, in *Monte Carlo and Molecular Dynamics Simulations in Polymer Science*, edited by K. Binder (Oxford University Press, New York, 1995) pp. 47-124.
15. T. Kreer, J. Baschnagel, M. Müller, K. Binder, *Macromolecules* **34**, 1105 (2001).
16. M. Doi, *Macromolecules* **17**, 2846 (1984).
17. M. Rubinstein, *Phys. Rev. Lett.* **59**, 1946 (1987).
18. J. des Cloizeaux, *Europhys. Lett.* **6**, 475 (1988); *Macromolecules* **23**, 4678 (1990); **25**, 841 (1992).
19. J.M. Deutsch, *Phys. Rev. Lett.* **54**, 56 (1985); *J. Phys. (Paris)* **48**, 141 (1987).
20. A.N. Semenov, *Physica A* **171**, 517 (1991).
21. A.N. Semenov, in *Theoretical Challenges in the Dynamics of Complex Fluids*, edited by T. McLeish (Kluwer, Dordrecht, 1997) pp. 63-86.
22. A.N. Semenov, M. Rubinstein, *Eur. Phys. J. B* **1**, 87 (1998).
23. H.P. Deutsch, K. Binder, *J. Chem. Phys.* **94**, 2294 (1991).
24. M. Müller, K. Binder, *Comput. Phys. Commun.* **84**, 173 (1994); *Macromolecules* **28**, 1825 (1995).
25. I. Carmesin, K. Kremer, *Macromolecules* **21**, 2819 (1988).
26. M. Wolfgang, J. Baschnagel, K. Binder, *J. Phys. I* **5**, 1035 (1995).
27. H. Weber, W. Paul, *Phys. Rev. E* **54**, 3999 (1996).